




# Photonic Spiking Neural Networks and Graphene-on-Silicon Spiking Neurons

Aashu Jha , Chaoran Huang , Hsuan-Tung Peng , Bhavin Shastri, *Senior Member, IEEE*,  
and Paul R. Prucnal, *Life Fellow, IEEE*

(Invited Paper)

**Abstract**—Spiking neural networks are known to be superior over artificial neural networks for their computational power efficiency and noise robustness. The benefits of spiking coupled with the high-bandwidth and low-latency of photonics can enable highly-efficient, noise-robust, high-speed neural processors. The landscape of photonic spiking neurons consists of an overwhelming majority of excitable lasers and a few demonstrations on nonlinear optical cavities. The silicon platform is best poised to host a scalable photonic technology given its CMOS-compatibility and low optical loss. Here, we present a survey of existing photonic spiking neurons, and propose a novel spiking neuron based on a hybrid graphene-on-silicon microring cavity. A comparison among a representative sample of photonic spiking devices is also presented. Finally, we discuss methods employed in training spiking neural networks, their challenges as well as the application domain that can be enabled by photonic spiking neural hardware.

**Index Terms**—Neural networks, nonlinear photonics, photonic integrated circuits.

## I. INTRODUCTION

ARTIFICIAL intelligence relies on neural networks, which are getting increasingly computationally intensive and power hungry: the computational power required by neural network models has doubled every 3.4 months in the last decade while the electronic hardware density has doubled every 2 years as per the Moore's law [1]. The need for energy-efficient neural processing has inspired neural hardware engineering, as conventional computers are intrinsically inefficient for distributed processing algorithms [2]. Building a neural hardware in electronics

Manuscript received July 28, 2021; revised December 9, 2021 and January 13, 2022; accepted January 19, 2022. Date of publication January 27, 2022; date of current version May 2, 2022. This work was supported by the Office of Naval Research (ONR)–Award No. N00014-18-1-2297. (A. Jha and C.Huang contribute equally to this work.) (Corresponding author: Aashu Jha.)

Aashu Jha, Hsuan-Tung Peng, and Paul R. Prucnal are with the Department of Electrical and Computer Engineering, Princeton University, Princeton, NJ 08544 USA (e-mail: aashuj@princeton.edu; hpeng@princeton.edu; prucnal@princeton.edu).

Chaoran Huang is with the Department of Electrical and Computer Engineering, Princeton University, Princeton, NJ 08544 USA, and also with the Chinese University of Hong Kong, Shatin 999077, Hong Kong (e-mail: chaoranh@princeton.edu).

Bhavin Shastri is with the Department of Physics, Engineering Physics and Astronomy, Queen's University, K7L 3N6 Kingston, ON, Canada, and also with the Vector Institute, Toronto, ON, Canada (e-mail: bhavin.shastri@queensu.ca).

Color versions of one or more figures in this article are available at <https://doi.org/10.1109/JLT.2022.3146157>.

Digital Object Identifier 10.1109/JLT.2022.3146157

TABLE I  
QUALITATIVE COMPARISON BETWEEN SPIKING NEURAL NETWORKS (SNNs)  
AND ARTIFICIAL NEURAL NETWORKS (ANNs)

	ANNs	SNNs
Energy consumption	Continuous	At firing events
Noise robustness	Low	High
Datasets	Static	Dynamic
Application domain	Non event-based eg image classification	Event-based (temporal) eg. time-series prediction
Training	Relatively easy	Hard

is bottlenecked by the deceleration of the Moore's law, as well as the fundamental tradeoff between bandwidth and interconnectivity [2], [3]. This deficiency of electronic hardware has spurred extensive research interest and engendered the nascent field of neuromorphic photonics that aims at leveraging the advantages of optics and neuromorphic architecture to enable a computing platform with high efficiency, interconnectivity and extremely high bandwidth [2], [4].

The vast landscape of neural network models can be broadly divided into artificial neural networks (ANNs), comprised of continuous-valued nonlinear activation functions operating on analog, static inputs, and spiking neural networks (SNNs) which operate on discrete spatiotemporal spikes. A summary of qualitative relative comparison of ANNs and SNNs is presented in Table I. Since spiking neurons are only active under a spike event, unlike ANNs that continuously process redundant information, the power consumption of SNNs can be significantly lower relative to ANNs [5]–[7]. The spiking nature of SNNs also results in superior robustness to input noise. Additionally, the temporal dimension gives SNNs a higher representational capacity making them computationally more powerful than their ANN counterparts [8], [9]. These features make SNNs perfect for event-based applications where temporally varying information is to be processed, e.g. time-series prediction and classification tasks. Of course, a practical realization entails a spiking neural hardware that can enable the theoretical power-efficiency and computational superiority of SNNs. Major implementations of spiking hardware in electronics include Loihi from Intel [10], Neurogrid from Stanford [11], TrueNorth from IBM [12], etc. Photonics i.e. optical physics offers a viable route to further push the energy efficiency and processing speed of SNNs.

Existing photonic spiking hardware are overwhelmingly based on excitable semiconductor lasers on III-V platforms

[13]–[17], which undergo high optical loss due to weak confinement of light and high material absorption, and can be prohibitive to scaling. Such scalability issues can be resolved by a silicon photonic platform, which is CMOS-compatible and benefits from existing fabrication technology, and have very low loss at telecom wavelengths. There has been some recent work in realizing spiking neuron functionality on silicon; most notably Refs. [18], [19] use phase-change materials embedded on silicon and silicon nitride platforms to engineer spiking-like functionality through nonlinear pulse transformation. However, the spiking behavior in their approaches is reliant on a synchronized operation between the output spike pulses and the input data. Their approaches face two fundamental limitations: the lack of temporal encoding feature, which is a key characteristic of spiking, and the lack of asynchronicity prohibits arbitrary network configurations. In this paper, we propose a CMOS-compatible spiking neuron based on a graphene-on-silicon nonlinear microring resonator where the nonlinear effects in silicon and graphene generates a spiking dynamical system. Graphene enhances the efficiency of the nonlinear photonic processes [20]–[22] that enables spiking at a much faster timescale ( $\approx$ picoseconds) previously impossible with silicon-only nonlinear devices [23], [24]. Additionally, spiking on a standard CMOS-compatible commercially-available silicon photonics (SiPh) platform offers the advantages of large-scale manufacturing and easy interface with standard silicon photonic components. While graphene-based integrated photonic technology has not matured quite as much as SiPh yet, the incredible performance merits of various graphene-based photonic devices should inevitably push for standardization of graphene integration on Si photonics [25]. It is thus timely to innovate in novel graphene-on-silicon devices.

Another crucial component of realizing an efficient neural network besides hardware is algorithms. ANNs have gathered mass acceptance due to their simplicity in training and availability of large labelled datasets. ANNs can learn on gradient-descent based algorithms like backpropagation [26], whereas SNNs require specialized algorithms due to the non-differentiable nature of spiking [27], [28]. The constraints become further stringent when it comes to a photonic hardware, which is highly susceptible to process variations and noise, and necessitates algorithm-hardware co-design. While training algorithms for spiking can be adapted from neuroscience and electronics, it will be key to be mindful of the requirements of photonic hardware and the application when selecting an algorithm.

Once there is a framework for spiking neural hardware and algorithms in place, it is also advantageous to evaluate the spike-based processing on event-based applications that naturally fall within the realms of spike-based processing. This goes against the approach that has been taken so far of chasing ANNs over classification accuracy. Event-based applications like brain-machine interfaces, autonomous driving etc, that also demand ultra-fast and low-power computation and are beyond the grasp of ANNs and spiking electronics are where we should deploy photonic spiking hardware. Availability of large dynamic datasets of such applications will be useful for efficient training before deployment.

In this paper, we provide a survey of existing demonstrations of photonic spiking neurons, propose a novel CMOS-compatible

spiking neuron design based on a graphene-on-silicon microring resonator and compare a representative sample of neurons against various performance metrics. We then summarize various training methods available to spiking neurons, show a simulated benchmark classification on our proposed neuron using one such class of algorithm and argue the case for local learning algorithms for photonic hardware. We finally discuss the application domain of spiking neural hardware that can best showcase their computational strength.

## II. OVERVIEW OF PHOTONIC SPIKING NEURONS

Existing demonstrations of photonic spiking neurons mirror biological neurons the closest in behavior rather than emulating them. Research in neuroscience has led to various models of biological neurons, encompassing a wide range of complexity from the earliest ones like the Hodgkin-Huxley model, which was computationally complex, to progressively simplified ones like the Izhikevich neuron model and then the leaky integrate-and-fire model. Developing a neural hardware entails replicating a given model's behavior. Laser cavities have long been studied for excitable and spiking properties [29]–[34]. However, the work of Nahmias *et al.* [14] drawing parallel between semiconductor lasers and the leaky *integrate-and-fire* neuron model rekindled interest in photonic spiking hardware. Consequently, an overwhelming majority of photonic spiking neurons are based on semiconductor lasers, while the remainder are variants of nonlinear optical cavities. One way to systematically categorize them can be to distinguish depending on whether the operation mechanism is opto-electronic or all-optical. Fig. 1 illustrates the categories, including a cartoon illustration of a representative system in each sub-category.

### A. Opto-Electronic Systems

This class of spiking systems includes semiconductor lasers where optical feedback within the laser cavities leads to nonlinearities that endow excitability. Refs. [3], [35] offer an exhaustive overview of the spiking neurons that fall under this class. The lasing mechanism is based on electrical pumping while the injection can be either electrical or optical. The electrically pumped devices are often studied with the Yamada model, which was first used to demonstrate excitability in lasers with saturable absorbers [31]. Notable examples within this include: graphene excitable laser [36], VCSELs [14], semiconductor optical amplifiers [37] and distributed feedback laser [35]. An illustrative operating principle of a distributed feedback laser is shown in Fig. 1 where the weighted optical signal is summed by a photodetector which drives the excitable laser resulting in output spikes.

The second class of spiking neurons based on optoelectronic lasers includes lasers that are optically injected i.e. the optical signal directly drives the excitable laser resulting in a spike response, as shown in Fig. 1. Early demonstration of excitability in lasers subject to optical injection was shown in [33], [38]. This was followed by excitable devices involving quantum dots [39], microring lasers [40], [41], microdisk lasers [42] and quantum wells [43].

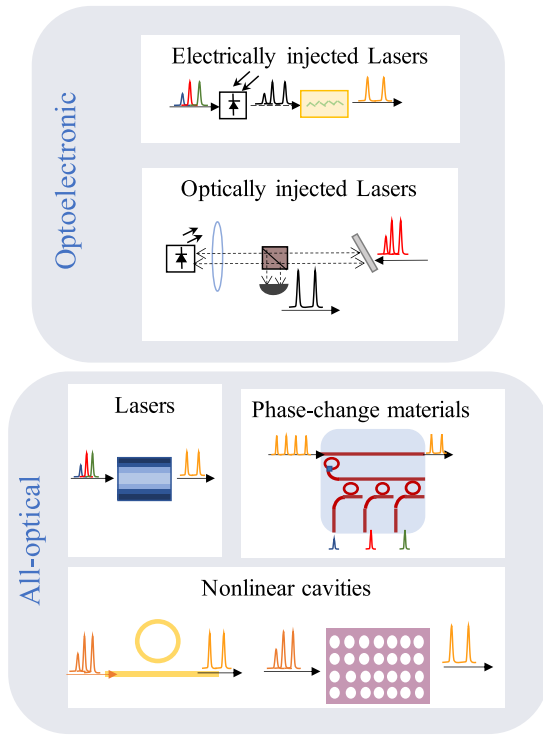


Fig. 1. Implementations of photonic spiking neurons, categorized into (top) optoelectronic devices including semiconductor lasers, and (bottom) all-optical devices, including lasers, phase-change material-based devices and nonlinear cavities. Additionally, the operational principles of each class of devices is also illustrated, showing incoming and output spikes, where colors represent optical wavelengths.

### B. All-Optical Systems

All-optical excitable devices have relatively more diversity in their operational principles, ranging from lasers to passive optical cavities to exotic material-enhanced cavities, as shown in Fig. 1. Lasers within this category include those that are optically pumped and become excitable in response to optical perturbations. Early works of this kind were done in Q-switched lasers [44] and lasers with saturable absorber [45], [46]. This was followed by several implementations of vertical cavity surface emitting lasers (VCSELs) [16], [17]. There was a parallel effort in studying all-optical excitability in optical cavities such as microring resonators [23] and photonic crystal cavities [24]. Recently there have also been substantial efforts towards realizing engineered excitability using phase change materials [18], [19].

Laser-based systems face the issue of scalability as their epitaxial and structural characteristics require non-standard specialized fabrication methods. On the other hand, integrated devices that can be fabricated at scale in a commercial foundry process has significantly higher odds of becoming a viable technology. Additionally, photonic fabrication technology is highly susceptible to process variation, and almost always requires electronics-assisted post fabrication compensation e.g. tuning resonator resonance wavelengths. This need for co-existing photonics and electronics requires photonics to remain compatible to CMOS electronics. These reasons together advocate for spiking neurons on CMOS compatible platforms like silicon. Prior

demonstrations of a CMOS-compatible spiking neuron either suffer from speed bottlenecks, or lack the asynchronicity fundamental to spiking neurons. In the following section, we propose an alternative approach of engineering a CMOS-compatible spiking neuron.

### III. A CMOS-COMPATIBLE SPIKING NEURON

In this section, we first present our nonlinear coupled-mode theory based model incorporating the nonlinear effects in silicon and graphene, and the basis of excitability in the microring. All-optical devices based on microrings have been previously used for optical memory [47], [47], switching [48], thresholding [49], pulse carving [50], etc. Using this model, we then show the simulation results showing key characteristics of a spiking neuron in a graphene embedded silicon microring cavity. These include: asynchronous spike generation in response to input perturbation, threshold operation, temporal integration, and cascability.

Excitability, and consequently spiking, in our device arises from silicon's nonlinear optical effects [51]. Similar approaches have been undertaken before: Ref. [23] demonstrated excitability through competing thermal and free-carrier dynamics, but the processing speed was capped to the MHz range due to the slower timescale of thermal effects. For excitability at higher speeds, faster mechanisms such as free-carrier and instantaneous Kerr effects can be used. However, such a fast excitable system has not yet been experimentally demonstrated due to the high optical power threshold to enter such a nonlinear regime [52]. We address this issue by incorporating graphene in the nonlinear dynamical system. Our proposed spiking neuron is based on a hybrid graphene-embedded silicon microring resonator (MRR). Graphene has previously been utilized for enhancing efficiency in several nonlinear silicon devices [20]–[22]. In [21], the authors even show a power threshold reduction of 50 times in a graphene-si cavity over just monolithic silicon. The combination of the MRR cavity-induced coherent power buildup and the enhancement of silicon nonlinearities by graphene improves the overall power efficiency of the fast excitability as compared to just silicon.

#### A. Coupled Mode Theory Model for the Hybrid Microring

A variety of photonic nonlinear effects are at play in a hybrid silicon-graphene microring cavity which together form the basis of the spiking dynamical system. A good introduction to silicon photonic nonlinearities can be found in [51], and the major effects in integrated silicon waveguides are shown in Fig. 1 of Ref. [53]. Due to the centrosymmetry in silicon crystalline structure, the nonlinear effects of interest are the first- and the third- order effects. The third-order nonlinear effects are instantaneous parametric processes and manifest as intensity-dependent dispersion, known as the Kerr effect, and absorption called two-photon absorption (TPA). TPA generates free-carriers that trigger first-order nonlinear effects namely, free carrier absorption (FCA) and dispersion (FCD). The free-carrier effects tend to be much stronger than the third-order effects in integrated SOI [51]. All the absorption mechanisms contribute

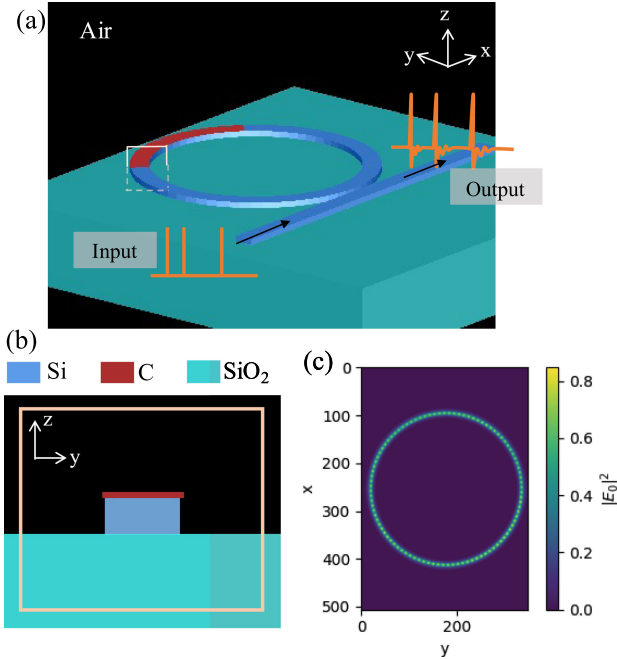


Fig. 2. (a) Perspective view of the hybrid graphene-on-silicon microring (MRR) coupled with a silicon bus waveguide. (b) YZ cross-section of the microring showing graphene overlaid on silicon. (c) Normalized electric field intensity,  $|E_0|^2$  profile of the resonant TE mode ( $\lambda = 1.555 \mu\text{m}$ ) at a midsection of the waveguide, as calculated by 3D FDTD solver on Lumerical. The simulation design parameters are: MRR radius =  $5 \mu\text{m}$ , waveguide height =  $220 \text{ nm}$ , width =  $500 \text{ nm}$ .

to thermal nonlinearity, which is a slow ( $\mu\text{s}$ ) dispersive effect and can be assumed to be constant for fast (GHz) signals. Kerr and thermal effects cause a red-shift in the cavity resonance while FCD causes a blue-shift. This is why FCD and Kerr effects are generally considered to be competing effects in nonlinear signal processing. Graphene also exhibits the third-order Kerr and TPA effects, and a strong first-order absorptive effect, known as saturable absorption. There are two main reasons as to why graphene can enhance efficiency of nonlinear silicon photonic effects. First, the Kerr effect in graphene is much higher than the silicon Kerr effect, and it acts in the same direction as the silicon FCD effect [54]. Thus the Kerr effect in graphene amplifies the FCD effect in silicon. Second, the saturable absorption in graphene induces a nonlinear dependence of the cavity quality factor on intensity, which facilitates nonlinear effects and reduces the power threshold for bistability [54].

To trigger the aforementioned nonlinearities, a microring resonator (MRR) is used to allow for coherent optical intensity buildup. A perspective view of the graphene-on-silicon MRR studied in this work can be found in Fig. 2(a) and a cross-section of the MRR waveguide is shown in Fig. 2(b). The dimensions of the microring are given in Table II. The high refractive index of silicon allows for strong light confinement to facilitate light-matter interaction in both silicon and graphene. Using a 3D finite-difference time domain (FDTD) simulation on Lumerical, the electric field distribution of the resonant TE mode of the microring coupled to a bus waveguide was calculated. Electric field intensity at the waveguide mid-section is shown

TABLE II  
SIMULATION PARAMETERS USED IN THIS WORK

Parameter	Value	Parameter	Value
$n_{2,\text{Si}}$	$4.5 \times 10^{-18} \text{ Wm}^{-2}$ [62]	R	5e-6
$n_{2,\text{G}}$	$-1 \times 10^{-13} \text{ Wm}^{-2}$ [63]	$W_{\text{Si}}$	500 nm
$\beta_{2,\text{Si}}$	$9 \times 10^{-8}$ [62]	$H_{\text{Si}}$	220 nm
$\tau_{\text{SA}}$	20 ps	$\tau_{\text{car}}$	20 ps
$\sigma_{\text{FCA}}$	$1.45 \times 10^{-23}$ [58]	$Q_0$	60e3
$I_{\text{sat}}$	$10^{10}$ [64]	$Q_e$	10e3
$\sigma_{r1}$	$8.8\text{e-}28 \text{ m}^3$ [65]	$n_{\text{Si}}$	3.478
$\sigma_{r2}$	$1.35\text{e-}22 \text{ m}^3$ [65]	$n_{\text{SiO}_2}$	1.44

in Fig. 2(c). We model light propagation in the microring using a nonlinear coupled-mode theory approach based on [55], with the inclusion of graphene contributions, i.e. its Kerr effect and saturable absorption in our updated model. The coupled ordinary differential equations for the temporal evolution of normalized cavity light amplitude  $a$  and free-carrier density  $n$  are given in (1) and (2):

$$\delta a / \delta t = \sqrt{P} + i(\delta a - n_{\text{kerr}}|a|^2 a) + i(n + \sigma_{\text{FCD}} n^{0.8}) a - (1 + \gamma_{\text{FCA}} n) a - \alpha_{\text{TPA}} |a|^2 a - \left( \frac{1}{1 + \frac{|a|^2}{W_{\text{sat}}}} \right) a \quad (1)$$

$$\delta n / \delta t = -\frac{n}{\tau} + |a|^4 \quad (2)$$

The time variable  $t$  is normalized with respect to  $\frac{1}{\Gamma_0}$  where  $\Gamma_0 = \omega_0 / 2Q_L$  where  $\omega_0$  is the microring resonance frequency, and  $Q_L$  is the loaded quality factor, which includes contributions from microring radiation loss, coupling loss and saturable absorption loss in the low-intensity limit in graphene. The cavity energy variable is normalized as  $|a|^2 = |u|^2 \sqrt{\sigma\beta}$ , where  $u$  is the unnormalized cavity mode energy and  $\sigma = \sigma_{r1} \frac{\omega_0}{n_0 \Gamma_0}$  and  $\beta = \frac{c^2 \beta_{2,\text{Si}}}{\Gamma_0 2\hbar\omega_0 n_0^2 V_{\text{TPA}} V_{\text{car}}}$ . where  $\beta_{2,\text{Si}}$  is the TPA coefficient of silicon. All the cavity nonlinear parameters calculated in (3)–(8) were obtained from the cavity field profile,  $E_0(r)$ , shown in Fig. 2(c).  $V_{\text{TPA}}$  is the nonlinear TPA volume parameter defined as per Ref. [56]; it quantifies the overlap of light and the nonlinear silicon material, and was calculated using (3):

$$V_{\text{TPA}} = \frac{\int n(r)^2 |E_0(r)|^2 d^3 r}{\int \beta(r) n(r)^2 |E_0(r)|^4 d^3 r} \quad (3)$$

Here  $\beta(r)$ ,  $n(r)$  and  $E_0(r)$  are spatially dependent variables.  $E_0(r)$  and  $n(r)$  were obtained from the FDTD simulation for the resonant fundamental TE mode where the integration volume is defined over a 3 d grid overlaying the microring. We set  $\beta(r) = \beta_{2,\text{Si}}$  for when  $n = 3.48$ , i.e. within the silicon waveguide. A two-dimensional cross-section of the resonant mode profile is shown in Fig. 2(c). Similarly,  $V_{\text{car}}$  is the nonlinear carrier volume, which was calculated as  $V_{\text{car}} = 2\pi R L_D$ , where  $R$  is the microring radius and  $L_D$  is the carrier diffusion length which is approximate as the waveguide width, similarly as Ref. [56].

In the first equation,  $P$  corresponds to the input light power, and is normalized as  $P = \frac{\sigma\beta\Gamma_c}{\Gamma_0} P_{\text{in}}$  where  $P_{\text{in}}$  is the input light power and  $\Gamma_c$  is the coupling coefficient between the bus waveguide and the microring. The imaginary terms on the right hand

side relate to the linear and nonlinear dispersive effects such as the Kerr and FCD effects.  $\delta$  is the normalized frequency detuning between microring resonance frequency and the input light wavelength.  $n_{\text{kerr}}$  contains the Kerr contributions of both silicon and graphene, and is defined in (4):

$$n_{\text{kerr}} = \frac{1}{\sqrt{\sigma\beta}\Gamma_0} (\gamma_{\text{kerr}}^{\text{Si}} + \gamma_{\text{kerr}}^{\text{G}}) \quad (4)$$

where the  $\gamma_{\text{kerr}}^{\text{Si}}, \gamma_{\text{kerr}}^{\text{G}}$  parameters are defined as per (5), (6):

$$\gamma_{\text{kerr}}^{\text{Si}} = \frac{\omega_0 c n_{2,\text{Si}}^{\text{max}}}{V_{\text{kerr}}^{\text{Si}}} \quad (5)$$

$$\gamma_{\text{kerr}}^{\text{G}} = \frac{\sigma_{3,\text{Im}}^{\text{max}}}{V_{\text{kerr}}^{\text{G}} \epsilon_0^2} \quad (6)$$

$n_{2,\text{Si}}^{\text{max}}$  is the Kerr coefficient of silicon and  $\sigma_{3,\text{Im}}^{\text{max}}$  is the third-order nonlinear conductivity of graphene which quantify the strength of the Kerr nonlinearity in each material.  $\sigma_{3,\text{Im}}^{\text{max}}$  is calculated using  $n_{2,\text{G}}^{\text{max}}$  for a graphene layer thickness of 0.33 nm [57], [58].  $V_{\text{kerr}}^{\text{Si}}$  and  $V_{\text{kerr}}^{\text{G}}$  are nonlinear Kerr volumes which measure the overlap between light and silicon and graphene respectively. They are defined as per the definition in Ref. [56], given in (7), (8) below:

$$V_{\text{kerr}}^{\text{Si}} = \frac{(\int n(r)^2 |E_0(r)|^2 d^3r)^2 n_2}{\int n_2(r) n(r)^2 |E_0(r)|^4 d^3r} \quad (7)$$

$$V_{\text{kerr}}^{\text{G}} = \frac{(\int n(r)^2 |E_0(r)|^2 d^3r)^2 \sigma_{3,\text{Im}}^{\text{max}}}{\int \sigma_{3,\text{Im}}(r) |E_{0,\parallel}(r)|^4 d^3r} \quad (8)$$

$V_{\text{kerr}}^{\text{Si}} = V_{\text{TPA}}$  as the nonlinear volumes primarily rely on the confinement of light in the nonlinear material rather than the magnitude of the nonlinear parameter itself.

The second term in the RHS of (1) corresponds to the free-carrier dispersion, where the  $\sigma_{\text{FCD}}$  term is defined as per Ref. [55], i.e.  $\sigma_{\text{FCD}} = \frac{\omega_0 \sigma_{r2}}{n\Gamma_0 \sigma^{0.8}}$ . The real parts of the RHS of (1) encompass the loss mechanisms: linear loss, free-carrier dependent loss ( $\gamma_{\text{FCA}}$ ) and two-photon absorption  $\alpha_{\text{TPA}}$ , which are defined as (9), (10):

$$\alpha_{\text{TPA}} = \frac{\beta_2 c^2}{2n^2 \Gamma_0 V_{\text{TPA}} \sqrt{\sigma\beta}} \quad (9)$$

$$\gamma_{\text{FCA}} = \frac{\sigma_{\text{FCA}} c}{2N\Gamma_0 \sigma} \quad (10)$$

The last term in (1) accounts for the intensity-dependent saturable absorption in the graphene layer, which is derived from the saturable absorption lifetime model given in Ref. [54].  $W_{\text{sat}}$  is the total stored energy in the cavity at the onset of saturable absorption, and is calculated as  $W_{\text{sat}} = (E_{\text{sat}}/E_{\parallel})^2$  where  $E_{\parallel}$  is the normalized electric field component tangential to the graphene layer and  $E_{\text{sat}} = \sqrt{2\eta_0 I_{\text{sat}}}$  where  $I_{\text{sat}}$  is the saturation intensity.

In (2) models the temporal evolution of normalized carrier density in the microring.  $\tau = \tau_{\text{car}} \Gamma_0$  is the normalized free-carrier lifetime in the cavity. Its dependence on  $|a|^4$  alludes to the TPA-mediated generation of free-carriers. Therefore our model in (1) and (2) encompasses all the nonlinear effects that occur in the hybrid graphene on silicon microring cavity. The

parameter values used in our simulation are tabulated in Table II. Parameters were either taken from the reference cited in the table, or specific to the simulated design.

### B. Analogy of the CMT Model to the Spiking Neuron Model

The simplest spiking neuron model that emulates the biological neuron behavior is the *integrate-and-fire* model. Its computational efficiency has made it the most popular model studied in computational neuroscience. (11) represents a simplified version of this model, where for the  $i$ th neuron of the network,  $y_i$  is the neuron state variable,  $a_i$  corresponds to the resting state,  $b_i$  is the internal neuron parameter,  $\delta$  corresponds to the spikes from connecting neurons with  $s_{ij}$  representing the synaptic connections.

$$\dot{y}_i = a_i + b_i y_i + \sum_{j=1}^n s_{ij} \delta(t - t_j^*) \quad (11)$$

An analogue to the *integrate-and-fire* model is the *resonate-and-fire* model proposed in Ref. [63]. Eq 12 describes this neuron model, which closely resembles (11). Here,  $z_i$  is the neuron state variable,  $\delta$  corresponds to the spikes from connecting neurons with  $c_{ij}$  representing the synaptic connections akin to the  $y_i$ ,  $\delta$  and  $s_{ij}$  terms in the *integrate-and-fire* model. The only difference is in the internal neuron parameter,  $(i\omega_i + b_i)$ , which has an imaginary component. This imaginary parameter introduces oscillatory dynamics in the neuron that is absent in *integrate-and-fire* neurons.

$$\dot{z}_i = (i\omega_i + b_i) z_i + \sum_{j=1}^n c_{ij} \delta(t - t_j^*) \quad (12)$$

Now we draw the analogy between our coupled-mode theory model of the microring and the *resonate-and-fire* model described in (12). To this end, we simplify (1) which describes the evolution of the neuron state variable,  $a$  i.e. the light amplitude in the microring. Eq 13 is a simplified version of (1).

$$\dot{a}_i = (i\Theta_i + B_i) a_i + I_i \quad (13)$$

The parameters introduced above are defined as follows:

$I_i = \sqrt{P}$ , corresponds to the input,  $B_i = 1 + \gamma_{\text{FCA}} n - \alpha_{\text{TPA}} |a|^2 - \frac{1}{1 + \frac{|a|^2}{W_{\text{sat}}}}$ , represents the amplitude decay mechanisms and  $\Theta_i = \delta - n_{\text{kerr}} |a|^2 + n + \sigma_{\text{FCD}} N^{0.8}$  represents the dispersive contributions. Comparing (12) and (13) clarifies the analogy between the two models.  $I_i$  is equivalent to the cumulative input term  $\sum_{j=1}^N c_{ij} \delta(t - t_j^*)$ . Similarly,  $(i\Theta_i + B_i)$  is functionally equivalent to the internal neuron parameter term,  $(i\omega_i + b_i)$ . As we investigate the dynamics of our neuron model in the following subsections, we will witness the oscillatory dynamics introduced in the system by the  $\Theta$  term, as is characteristic of *resonate-and-fire* neurons.

### C. Steady-State Characteristics

The first step to emulate a spiking neuron in the microring is to show excitable dynamics. Excitability occurs when a perturbation from a system's rest state results in a large excursion of

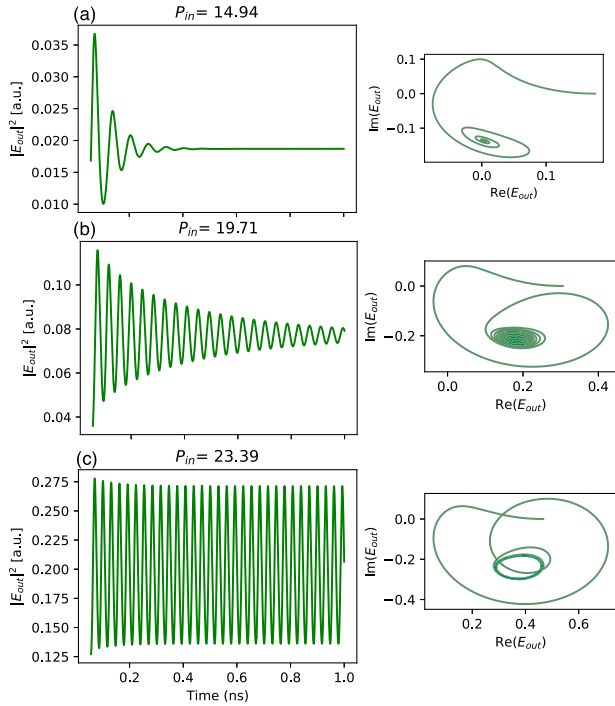


Fig. 3. Dynamics of characteristic class II excitability. (a)-(c) show the temporal evolution of output power and (i)-(iii) show the corresponding phase space portraits of cavity light amplitude ( $u$ ), in response to static input power to the MRR. The input power increases from top to bottom. The titles of (a)-(c) note the corresponding simulation parameters (normalized input power ( $P_{IN}$ ), normalized frequency detuning ( $\delta$ ), saturable absorption lifetime ( $\tau_{SA}$ ) and free-carrier lifetime ( $\tau_c$ ) in picoseconds).

physical variables, i.e. output light in our case, followed by an eventual rest back to the equilibrium. In [23], the authors show the existence of a class II excitable system in a silicon microdisk close to a regime of self-pulsation. Self-pulsation refers to the phenomenon where light oscillates between two output states in response to a constant input light power. In addition to Ref. [23], it has also been previously reported in several other photonic cavities [55], [64].

Motivated by their results, we look for a self-pulsation regime in our device. To do that, we characterize the temporal dynamics of output light in response to a continuous wave (CW) optical input by solving the ODEs in (1), 2. Fig. 3 shows the temporal evolution of output power,  $|E_{out}|^2$  in response to different input light powers,  $P_{in}$ , as well as the corresponding phase portraits of the output light amplitude,  $E_{out}$ . Fig. 3(a) shows that in a relatively low input power regime, the output light amplitude decays to a steady state and the corresponding phase portrait in the right plot shows decay to a stable fixed point. By increasing the input power further (Fig. 3(b)), the output undergoes damped oscillatory decay to a steady state, where the phase portrait reveals oscillations and slow decay to a fixed point. Finally, a relatively higher input power (Fig. 3(c)) results in a stable oscillating output, while in the phase portrait, a stable limit cycle is formed. This is the regime of self-pulsation, which results from the interaction between FCD-induced blue-shift of the microring resonance frequency and the light intensity in the MRR, much

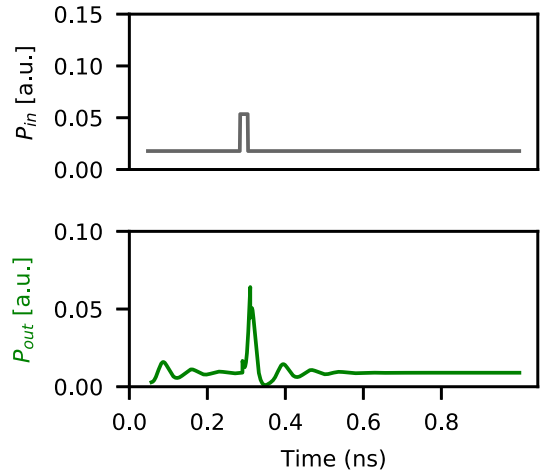


Fig. 4. Spiking behavior in the MRR. (top) Input light with perturbation, (bottom) corresponding output with a spike response to input perturbation.

like in [55]. The only difference is that in our case, graphene Kerr boosts the FCD effect, and the saturable absorption lifetime, which determines the photon cavity lifetime, ensures that the photon cavity lifetime is roughly the same order of magnitude as the free-carrier lifetime. Such a transition from decay to oscillatory decay to a stable oscillatory state is characteristic of a class II excitable dynamical system. Additionally, the oscillatory decay to steady state is indicative of a *resonate-and-fire* neuron behavior as discussed in the previous section.

#### D. Spiking Neuron Dynamics

Excitability in a spiking system is characterized by the following properties: 1. temporal integration of incoming pulses, 2. generation of a spike for inputs above a threshold, and 3. asynchronous spike generation without being triggered on input. These properties enable the repeatable nature of a spiking dynamical system that assures computational power efficiency and noise robustness. We shall investigate whether these properties exist in the hybrid microring system. Similar to [23], we look for excitability in proximity to the self-pulsating regime. More specifically, excitability in this case means for a constant input power slightly below the self-pulsation threshold, if there is a perturbation that crosses the self-pulsation threshold, it can throw the system into a limit cycle-like state resulting in an output spike. Fig. 4 shows a perturbed input, where the constant power level is below while the perturbation is above the self-pulsation threshold. The input perturbation results in an output spike. This illustrates the excitable property of the microring that results in spiking. Unlike the typical integrate-and-fire neurons [13], [15] where upon stimulation, the output undergoes an exponential decay to the rest state, here we find a damped oscillatory decay to the rest state. Such a damped oscillation is again reminiscent of resonate-and-fire neurons. To reiterate, the oscillatory dynamics results in resonate-and-fire neurons from the state variable being complex. Further discussion of resonate-and-fire neuron characteristics of the nonlinear microring will be presented later.

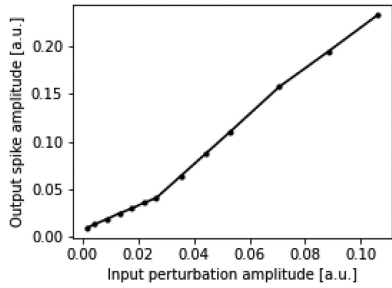


Fig. 5. Output spike amplitude as a function of input perturbation amplitude illustrating a threshold behavior.

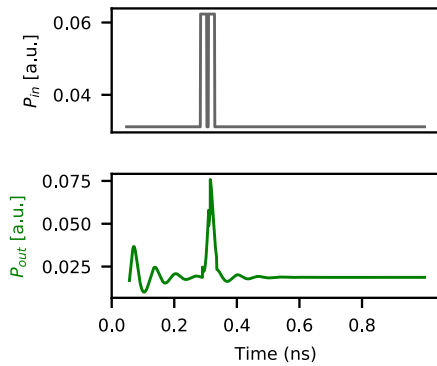


Fig. 6. Temporal integration. (top) Input pulse train, with closely spaced pulses, (bottom) Corresponding output showing a single spike.

The presence of a spiking threshold is evidenced in Fig. 5, which shows the output spike amplitude ( $P_{out}$ ) as a function of the input perturbation amplitude  $P_{in}$ . Unlike typical integrate-and-fire spiking neurons with a rectified linear unit (ReLU) like transfer function, the transfer function here has more of a leaky ReLU transfer function i.e.  $P_{out} \neq 0$  for  $P_{in}$  below the threshold. The equivalent pulse energy required for spiking, calculated by multiplying the input pulse power amplitude with its duration is about 0.7 pJ in this device. This fares well compared to photonic spiking neurons based on phase change materials in [18] where they report energy consumption per neuron of about 4 pJ. The energy consumption of an electronic spiking neuron e.g. Intel’s Loihi neuron was reported at about 80 pJ [10]. Our photonic spiking neuron thus fares well against the electronic approaches.

Another critical feature of a spiking neuron is temporal integration, which means the device response is proportional to the perturbation energy i.e. power integral within some temporal window. To check for this feature, we first study the device response to a doublet of closely spaced input pulses, each of whose amplitude is below the spiking threshold, shown in Fig. 6. The corresponding output shows a single spike in response to the input pulse doublet which illustrates that spike response is dependent on the total energy within the input pulse. We further investigate the temporal integration feature by varying the amplitude of the input pulse,  $|P_{in}|$  and measuring the time delay between the input pulse and the onset of output spike,  $\Delta T_{spike}$ . The results of this study with simulated data, and the corresponding polynomial fit, is shown in Fig. 7. The time

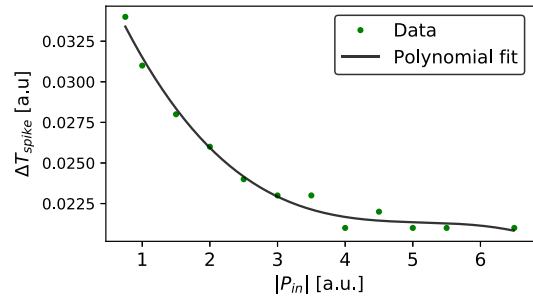


Fig. 7. Temporal Integration characteristics. Delay between starting edge of input pulse and onset of spike,  $\Delta T_{spike}$ , as a function of input pulse perturbation amplitude,  $|P_{in}|$ . Dots correspond to simulated points while the curve in black is a polynomial fit to the data showing decay of  $\Delta T_{spike}$  with increasing  $|P_{in}|$ .

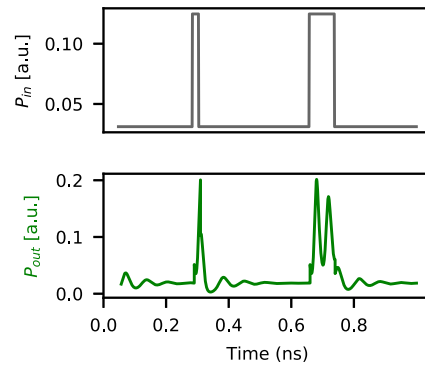


Fig. 8. Pulse energy encoding: (top) input pulse sequence with different pulse widths, (bottom) corresponding output spikes where the input pulse energy information is encoded into the number of output spikes.

delay is found to decay with increasing perturbation amplitude and eventually reach a constant floor. This is consistent with our expectation of an temporally integrating neuron – the initial decrease in  $\Delta T_{spike}$  is because increasing power means the threshold energy required to spike is reached sooner, however after a certain point, there is an intrinsic latency due to the cavity lifetime resulting in a low limit of  $\Delta T_{spike}$ .

While the property of temporal integration reveals that the microring encodes the energy within the input pulses, we further study the second-order property of pulse-energy encoding in the microring. We first characterize the system response to input pulses of different pulse widths shown in Fig. 8. In the short input pulse width limit (left pulse), the system responds with a singular spike. On the other hand, in the long pulse width limit (right pulse), the system generates a pulse doublet. We find that increasing the pulse width further results in bursts of spikes. With identical input peak power, the pulse width is a measure of the pulse energy; these results reveal the pulse energy encoding feature of the spiking dynamical system. Additionally, the ability of the system to generate spike bursts, where the inter-spike timing encodes input pulse information, is valuable for reliable synaptic transmission between neurons as well as selective activation [65].

To further verify the *resonate-and-fire* neuron characteristics of the microring, we investigate its response to the frequency of input pulses. In [63], such neurons are said to have an intrinsic

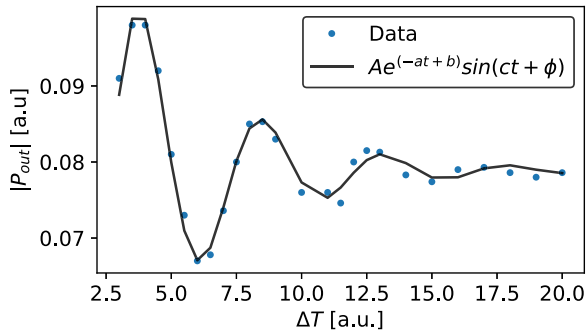


Fig. 9. Dependence of spike response on the input frequency. Amplitude of output spike,  $|P_{out}|$  as a function of time separation between two input pulses,  $\Delta T$ .

eigenfrequency and are thus sensitive to the frequency of the input pulses. We simulate the device response, quantified as the amplitude of the output spike,  $|P_{out}|$ , to input pulses of varying inter-pulse spacing,  $\Delta T$ . Fig. 9 shows the simulated data points with an overlaid damped oscillator fit function. We find a damped periodic oscillation in the output spike amplitude as a function of inter-pulse spacing. The oscillation decays in the long inter-pulse spacing regime. This periodicity suggests that the neuron response has some dependency on the input frequency, which is an expected characteristic of this class of neurons.

Another important characteristic of a spiking neuron to be networkable is cascability, which is the ability of a neuron to excite a subsequent neuron. A simple demonstration of this is to feed the output of a neuron ( $N_1$ ) to an identical neuron ( $N_2$ ) as input, and observe the response of  $N_2$ . We checked such a configuration in simulations, and found that  $N_2$  outputs a spike in response to spike output from  $N_1$ . This showed that an input perturbation is sufficient to trigger spike response and that the shape of the perturbation doesn't influence the output response. However, another important condition to satisfy is gain cascability, which means the ratio of the amplitude of output spike to the amplitude of input perturbation has to be  $\geq 1$ . This cannot be satisfied in an all-optical device with some inevitable optical loss. For a neuron with finite loss, the input power  $P_{in}$  required to trigger a spike response from  $n$  neurons diverges as  $n$  becomes large. While this may be an issue, there might be clever ways to circumvent around it – e.g. one can operate the neuron with two optical sources in a pump-probe scheme where one source provides the optical CW pump to each neuron, while the other the perturbation (or spike) from the previous neuron. This scheme of individually pumping each neuron can ensure the neuron is always operating close to the spiking threshold, which will permit operation of small networks. On-chip waveguide amplification can further supplement the optical powers for realizing larger scale systems [66]. This line of investigation will inform the future direction of this work.

#### IV. COMPARISON OF PHOTONIC SPIKING NEURONS

In this section, we will delve into the merits and drawbacks of various spiking neuron devices in the context of implementation in a large network. Of course the overall performance of the

TABLE III  
PERFORMANCE METRICS OF STATE-OF-THE-ART PHOTONIC SPIKING NEURONS

Device	Platform	Energy per pulse (pJ)	Firing rate [GHz]	Footprint [ $\mu\text{m}^2$ ]
DFB Laser [70]	InP	50	$\sim 2$	$> 600 \times 200$
Graphene laser [13]	InGaAsP-C-Si	75	4	40
Microdisk Laser [44]	InAsP-Si	0.2	1	25 $\pi$
RT-PD [71]	InGaAsP	50	0.11	600
VCSEL [16], [72]	Discrete	0.4	1	40,000
2D PhC [24]	InP	2	0.005	500
MRR [23]	Si	6	0.005	100
PCM-based cavity [18]	SiN	4	0.02	3600 $\pi$
Graphene-Si MRR	Si	0.7	40	100

network will depend on factors outside the neuron. Network architecture determines the number of interconnecting synapses, which scale quadratically with the number of neurons (in a fully-connected configuration). So for a large network, costs associated with synapses may overwhelm the overall network costs. However, here we limit our focus to spiking neurons themselves. To this goal, we have identified relevant performance metrics, such as energy consumption, neuron firing rate i.e. processing speed, latency and footprint. We compare a representative subset of optoelectronic and all-optical devices against these metrics as enlisted in Table III.

First, we compare the devices on a simple scale of physical size. This can be the primary constraint in edge computing devices. Integrated devices are naturally better than discrete ones in this regard as can be seen in Table III. Within integrated devices, platform-specific properties like optical material loss and refractive index further limit the footprint. Passive silicon-based devices tend to be the most compact due to the high index of silicon. Incidentally, these devices host all-optical spiking neurons. Additionally, electrical components, like photodetectors, interfacing optoelectronic devices can further add to their footprint.

The next consideration is firing rate, or alternatively, the processing speed of a spiking neuron. Firing rate determines the temporal resolution of the spike-based processing. High-speed ( $\geq$  GHz) processing is where neuromorphic photonics can really outshine electronics, which makes processing speed a major metric to consider. All-optical devices relying on slow nonlinear phenomena like thermal effects, are the slowest ones. Excitable lasers can operate up to a few GHz timescales. For higher speed needs, passive silicon-based all-optical graphene based neuron proposed in this work stands out as the most promising candidate.

Finally, we compare the energy consumption associated with the devices enlisted here. The values shown in Table III are either reported directly from the cited literature or calculated using the reported parameters. One could naively expect that optoelectronic devices have significantly lower energy costs than all-optical devices, considering the high-power requirements of nonlinear optical processes. However, once the cost of optoelectronic conversion is factored in, the difference is not as dramatic as one would expect. Among the devices shown in Table III, optoelectronic laser-based devices have higher energy requirements on average than all-optical ones. In principle, the energy consumption of cavity-based all-optical devices can further be reduced by implementing photonic cavities with smaller mode volumes like photonic crystals.



Overall it is fair to say that there is no ideal spiking device that beats everything else across all metrics. There are additional challenges in both optoelectronic as well as all-optical approaches to really portray the full picture. For optoelectronic devices, we did not consider the speed limits due to parasitics in electronic links that can bottleneck the neuron processing speed. This may be addressed by heterogeneous integration with a CMOS chip via flip-chip bonding [70] allowing for use for high-speed CMOS electronic components with a low parasitic pathway. Similarly, in all-optical devices, optical power cascading is a concern, as optical power is inevitably lost at each stage of the network. In the future, waveguide amplifiers [71] may alleviate these concerns by allowing for amplification every few stages.

## V. TRAINING SPIKING NEURAL NETWORKS

Training refers to adjusting synaptic weights in the process of optimizing for a cost function, which can correspond to the difference between the target and actual output of a neural network. In the context of artificial neural networks, neurons represent static, continuous-valued nonlinear activations that are differentiable, which means they can be trained using gradient-descent based supervised learning algorithms like error backpropagation [72]. In contrast, spike-based processors operate on dynamic temporal data that are an accumulation of delta function-like spikes that are non-differentiable, hence conventional backpropagation algorithms don't apply. Despite the touted benefits in energy-efficiency and noise robustness of SNNs relative to ANNs, the performance of SNNs on most machine learning tasks lag behind the ANNs primarily due to the issue of trainability [27], [72]. This is further aggravated by the scarcity of dynamic dataset compatible to SNNs in contrast to the availability of large labelled static datasets for ANNs. Of course this impediment to SNN has attracted a lot of interest from neuroscientists and computer scientists alike to develop training algorithms catered to spiking neural networks. These algorithms can broadly be classified into two categories:

- *Conversion-based algorithms*: this approach aims to leverage backpropagation methods in ANNs by training the network as an ANN and then converting to an SNN [73], [74]. Essentially, the static input (eg. pixel intensity in an image classification task) is converted to a spike train based on encoding schemes, such as rate encoding [75]. An activation function that functionally resembles that of a spiking neuron, such as a rectified linear unit, ReLU, is chosen. Once training is done, weights are normalized to avoid arbitrarily high firing rates and the spike output is converted back to a static, analog value using the complementary decoding scheme. The merit of this approach is that it circumvents the difficulties of training temporal signals and can use existing frameworks like TensorFlow [76] and Pytorch [77]. However, it suffers from the vanishing forward spike propagation problem where firing rates progressively decrease through network layers. Also, you pay for the training convenience in longer inference times owing to the conversion [27]. This approach has been

considered in photonic systems simulations – Ref. [78] show an MNIST image classification using a rate encoding approach. Ref. [79] even showed online rate encoding using a VCSEL based neuron.

- *Spike-based algorithms*: this approach attempts to train using temporal data, without any conversion, and thus benefits from the sparsity and efficiency of spiking neural networks. Neuroscientists have identified various learning rules, based on neuroplasticity in actual biological synapses, known as spike-timing dependent plasticity (STDP). In STDP, weight is adjusted in response to the relative time difference between spikes of the connecting neurons. It has been used for both supervised and unsupervised learning. The spatial and temporal locality of STDP endows network-level effects such as reduced latency. The early works used STDP to perform spike based learning in a supervised manner, examples include ReSuMe [80] and Tempotron [81]. STDP has been abundantly demonstrated in photonic systems, starting out in [82] to more recent implementations in VCSEL-based systems [83], [84], [85], [19]. More recent supervised algorithms mirror backpropagation by approximating a differentiable function as the spiking nonlinearity and using gradient-descent based algorithms to optimize for the target spike train. Examples include SpikeProp [86], NormAD [87]. There have been no implementations of such algorithms in photonic systems to the best of our knowledge. Typically, in software, unsupervised algorithms tend to have inferior performance over conversion-based supervised learning.

### A. Benchmark MNIST Handwritten Digit Classification Simulation

Here we employ a conversion-based algorithm to do a system-level analysis of our proposed spiking neuron. We simulate a three-layer fully-connected spiking neural network and study its accuracy in a benchmark MNIST handwritten digit classification task. The scheme is similar to typical artificial neural networks except the nonlinear units in the input and hidden layers are the spiking neuron units, and the inputs to the network are spike-based time series instead of analog values. This simulation is done using the Bindsnet simulation package [88] which allows simulating spiking neural networks within the Pytorch framework. The schematic of the network is shown in Fig. 10(a). Each input image in the MNIST dataset is composed of 28x28 pixels. First, each pixel in a given image is encoded using the Poisson encoding transform in Bindsnet and converted to a spike-based time series i.e. a format comprehensible by the spiking neurons. Fig. 10(b) shows the time series representation of the 784 pixels on the sample image. The frequency of the time series is proportional to the pixel intensity.

Each time series is then fed into an input layer with 784 (=28x28) neuron nodes. To emulate the spiking nonlinearity in each node, we employ the transfer function of the spiking neuron (shown in Fig. 5) as the nonlinear activation function. The input layer is fully connected to a hidden layer with 64 nodes,

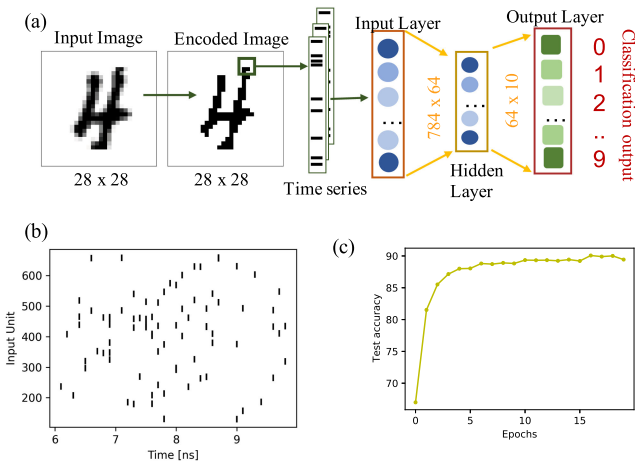


Fig. 10. Benchmark MNIST handwritten digit classification simulation using spiking nonlinear nodes. (a) Schematic of the simulated classification network, showing a sample MNIST dataset image being encoded into a time series, and fed into a 3 layer fully-connected network. (b) Time-series equivalence of the encoded image in (a): each row corresponds to the time-series for a given pixel in the input image. (c) Inference classification accuracy as a function of epoch count.

resulting in  $784 \times 64 = 50176$  trainable parameters. The hidden layer is subsequently fully-connected to an output layer with 10 nodes, corresponding to the 10 possible digit label outputs, resulting in additional  $64 \times 10 = 640$  trainable parameters. We use the log softmax function as the nonlinearity of the nodes in the output layer, which is typical for such multi-label classification networks.

At each time step, the input value for a given pixel is either a 1 or a 0 corresponding to the presence or absence of a spike event. The input time series propagates through the network, and results in an output neuron in the output layer to spike at the highest rate for a given image. Then this neuron is compared to the label associated with the image and a negative log likelihood loss is calculated. While training the network, a stochastic gradient descent-based optimizer (Adam) was used to minimize the loss.

In the inference stage, accuracy is computed by calculating the percentage of images that were correctly classified by the network. Fig. 10(c) shows the inference accuracy as a function of epochs, where the network is shown to converge to 93% accuracy in about 10 epochs. This result demonstrates the feasibility of using the proposed spiking neuron in a spiking neural network. Our simulated network is much smaller than the one proposed in a similar work [78], where 500 neurons were used in the hidden layer, although we achieved a slightly lower accuracy.

### B. Training in Photonics

As discussed earlier, training spiking neural networks in itself remains an unresolved problem. The challenges compound when we translate the problem into the context of photonics, where process variations and operational constraints can further aggravate performance. Nevertheless, photonics can benefit from advances in algorithm research within computer science or electronics community, but it will be critical to judge which

approach translates nicely to photonics. Here we present our outlook on the approaches to training photonic spiking neural networks.

Conversion-based training algorithms based on rate-encoding strategies have had better performance over spike-based ones for conventionally ANN-oriented tasks like classification. Due to the convenience of this approach and the availability of dataset for classification tasks, this will likely be the popular approach for researchers to demonstrate the functionality of their spiking devices in the near term. However, this approach only allows for offline training and online inference. And we are yet to see how this approach will pan out when actually implemented on a photonic hardware. Robust characterization of photonic devices can be expected to be incredibly difficult, which means the discrepancy due to variations in hardware operation will cause performance degradation during online inference. Additionally, the conversion steps will add to the inference time, which may eliminate applicability in real-time applications.

The ultimate way to ensure error-resilience to process variation and noise in photonics is online learning. Such approach can allow for algorithm-hardware co-design such that hardware-induced errors can be reliably mitigated. As discussed before, spiking hardware is not compatible with global learning rules like back propagation. Instead, to enable online learning in spiking hardware will require spatially local learning rules. Besides online learning, local learning allows leveraging the full potential of spiking networks, in terms of low inference latency. A common local learning rule in spiking, as we've discussed before, is STDP. STDP in photonic hardware have exclusively been shown in active platforms, using cross-gain modulation in SOAs [89], [90], vertical cavity SOAs (VC-SOAs) [84], [91]. As discussed earlier, for photonic spiking to be a viable technology, compatibility to CMOS is crucial. The singular proposal of implementing STDP on a passive photonics platform was in Ref. [92] using nonlinear optical effects. Ref. [19] used an STDP-like learning approach through a feedback loop mechanism. While STDP is amenable to local learning, it does not really optimize towards a global objective function, and has had lower accuracy when compared to back-propagation methods [93]. Higher performance may be obtained by using local learning rules that can allow for some form of global optimization through local weight update rules, akin to the Hopfield network that always seeks to minimize the global energy function. We thus foresee algorithms with local learning with a global optimization scheme to be the most suitable route when it comes to training photonic spiking hardware.

## VI. APPLICATION DOMAIN OF PHOTONIC SNNs

Most application-oriented works in spiking neural networks have resorted to classification tasks as a means to compete against artificial neural networks. However, due to the lack of adequate training algorithms for SNNs, they perform relatively poorly in terms of accuracy. SNNs are underutilized if limited to such classification cases; their temporal encoding feature is better suited to applications with sparse dynamic data. Sample applications include natural language processing, event-based

sensing and processing (high-speed navigation and localization: object tracking, scene reconstruction), etc. which would be prohibitive to carry out in conventional ANNs in an energy-efficient manner.

Event-based sensors output data in the form of spikes and spike-based processing naturally fits into the task of processing signals from such sensors. Applications within event-based sensing span tracking, robotics, object tracking, etc [28]. However, implementing application-oriented spike-based processing on a spiking hardware remains largely outstanding, except for a few works – Ref. [94] showed the use of TrueNorth, a spiking electronic hardware, for real-time gesture recognition from a dynamic vision sensor. There have not been any demonstrations of such applications in a spiking photonic hardware yet. The low-latency, high energy efficiency and processing speed of photonics makes it even more suitable for such applications. For instance, autonomous driving simultaneously requires low power and high speed processing, where conventional ANNs have significant computational overhead and latency [95]. Another application can be brain-machine interfaces since SNNs can process biological spikes without transformation and offer low energy consumption, low latency, low thermal dissipation as required by these systems [96]. Finally, the simultaneous high-speed and low power operation of spiking neurons can be beneficial for high-speed radio-frequency (RF) signal processing. Cognitive radio networks require high-speed decision making for resource allocation, and it has been shown in simulation that the spatio-temporal dynamics of spiking networks can enable such functionality [97].

Even with classification-like tasks, SNNs may enable continual learning that ANNs are incapable of [27]. In deep learning models based on continuous-valued neurons, the network adapts to new datasets, and forgets old patterns in the process. This is in stark contrast to the human brain where memory tends to be permanent, barring any injuries or disease. With the additional temporal dimension in SNNs, SNNs may potentially enable continual learning [27]. Applications beyond the reach of conventional ANNs and spiking electronics are the real opportunities where photonic spiking hardware can fully demonstrate its computational might.

## VII. CONCLUSION

Spiking neural networks offer the possibility of computationally powerful, noise-resilient next-generation neuromorphic processors. However, conventional computers are incompetent for such a distributed processing model which advocates for a specialized hardware. Electronics faces fundamental bottlenecks in interconnectivity and bandwidth, and presents an opportunity to capitalize on photonics. Innovations in developing photonic spiking hardware has lasted just over a decade, and we may now be at the cusp of enabling a real technological platform capable of real applications.

The landscape of photonic spiking neurons can broadly be classified into optoelectronic devices including excitable lasers and all-optical devices, including nonlinear photonic cavities. Laser-based devices on discrete or active platforms may not

be as conducive to scalability as the CMOS-compatible devices. To this end, we have proposed a novel spiking neuron design based on a graphene-on-silicon microring resonator. We have presented preliminary simulation results showing spiking neuron-like behavior of the microring device, which arises from the interplay of nonlinear optical effects in both graphene and silicon. While the exact architecture of the interfacing synapses is not clear yet, we expect it to be a coherent, i.e. single wavelength, device to ensure compatibility with the MRR neuron. It may be a waveguide or a mach-zehnder interferometer (MZI) with tunable absorptive or refractive elements using phase-change materials or metal heaters or graphene.

As we widen the lens from devices to systems based on photonic spiking hardware, we will need to consider algorithms that can optimize the performance of the network for a given application while ensuring resiliency to process variations and noise in hardware. Local online learning rules can be a good avenue for exploration that may be able to accommodate for the needs of photonic hardware. Finally, it is important to carve out the application space of photonic spiking neuron technology – likely outside the scope of ANNs and spiking electronics. These might include event-based sensing applications, autonomous control, etc. Only once photonic spiking neurons can enable applications beyond what was previously possible with spiking electronics or ANNs will they be worth the research efforts spent on them. The confluence of innovations in spiking neuron devices and in algorithms paints a hopeful future for what is ahead.

## REFERENCES

- [1] D. Amodei, "Ai and compute," *OpenAI*, 2021. [Online]. Available: <https://blog.openai.com/ai-and-compute>
- [2] B. J. Shastri *et al.*, "Photonics for artificial intelligence and neuromorphic computing," *Nature Photon.*, vol. 15, no. 2, pp. 102–114, 2021.
- [3] P. R. Prucnal, B. J. Shastri, T. F. de Lima, M. A. Nahmias, and A. N. Tait, "Recent progress in semiconductor excitable lasers for photonic spike processing," *Adv. Opt. Photon.*, vol. 8, no. 2, pp. 228–299, 2016.
- [4] P. R. Prucnal and B. J. Shastri, *Neuromorphic Photonics*. Boca Raton FL: CRC Press, 2017.
- [5] W. Maass, "Lower bounds for the computational power of networks of spiking neurons," *Neural Comput.*, vol. 8, no. 1, pp. 1–40, 1996.
- [6] W. Maass and H. Markram, "On the computational power of circuits of spiking neurons," *J. Comput. Syst. Sci.*, vol. 69, no. 4, pp. 593–616, 2004.
- [7] A. Amir *et al.*, "A low power, fully event-based gesture recognition system," in *Proc. IEEE Conf. Comput. Vision Pattern Recognit.*, 2017, pp. 7388–7397.
- [8] W. Maass, "Networks of spiking neurons: The third generation of neural network models," *Neural Netw.*, vol. 10, no. 9, pp. 1659–1671, 1997.
- [9] Y. Wu, L. Deng, G. Li, J. Zhu, and L. Shi, "Spatio-temporal backpropagation for training high-performance spiking neural networks," *Front. Neurosci.*, vol. 12, p. 331, 2018.
- [10] M. Davies *et al.*, "Loihi: A neuromorphic manycore processor with on-chip learning," *IEEE Micro*, vol. 38, no. 1, pp. 82–99, Jan./Feb. 2018.
- [11] B. V. Benjamin *et al.*, "Neurogrid: A mixed-analog-digital multichip system for large-scale neural simulations," *Proc. IEEE*, vol. 102, no. 5, pp. 699–716, May 2014.
- [12] F. Akopyan *et al.*, "Truenorth: Design and tool flow of a 65 mw 1 million neuron programmable neurosynaptic chip," *IEEE Trans. Comput.-Aided Des. Integr. Circuits Syst.*, vol. 34, no. 10, pp. 1537–1557, Oct. 2015.
- [13] B. J. Shastri, M. A. Nahmias, A. N. Tait, A. W. Rodriguez, B. Wu, and P. R. Prucnal, "Spike processing with a graphene excitable laser," *Sci. Rep.*, vol. 6, no. 1, pp. 1–12, 2016.
- [14] M. A. Nahmias, B. J. Shastri, A. N. Tait, and P. R. Prucnal, "A leaky integrate-and-fire laser neuron for ultrafast cognitive computing," *IEEE J. Sel. Topics Quantum Electron.*, vol. 19, no. 5, pp. 1–12, Sep./Oct. 2013, Art no. 1800212.

- [15] H.-T. Peng *et al.*, "Temporal information processing with an integrated laser neuron," *IEEE J. Sel. Topics Quantum Electron.*, vol. 26, no. 1, pp. 1–9, Jan./Feb. 2020, Art. no. 5100209.
- [16] A. Hurtado, K. Schires, I. Henning, and M. Adams, "Investigation of vertical cavity surface emitting laser dynamics for neuromorphic photonic systems," *Appl. Phys. Lett.*, vol. 100, no. 10, 2012, Art. no. 103703.
- [17] S. Barbay, R. Kuszelewicz, and A. M. Yacomotti, "Excitability in a semiconductor laser with saturable absorber," *Opt. Lett.*, vol. 36, no. 23, pp. 4476–4478, 2011.
- [18] I. Chakraborty, G. Saha, A. Sengupta, and K. Roy, "Toward fast neural computing using all-photon phase change spiking neurons," *Sci. Rep.*, vol. 8, no. 1, pp. 1–9, 2018.
- [19] J. Feldmann, N. Youngblood, C. D. Wright, H. Bhaskaran, and W. Pernice, "All-optical spiking neurosynaptic networks with self-learning capabilities," *Nature*, vol. 569, no. 7755, pp. 208–214, 2019.
- [20] A. Ishizawa *et al.*, "Optical nonlinearity enhancement with graphene-decorated silicon waveguides," *Sci. Rep.*, vol. 7, 2017, Art. no. 45520.
- [21] T. Gu *et al.*, "Regenerative oscillation and four-wave mixing in graphene optoelectronics," *Nature Photon.*, vol. 6, no. 8, pp. 554–559, 2012.
- [22] Q. Feng *et al.*, "Enhanced optical Kerr nonlinearity of graphene/Si hybrid waveguide," *Appl. Phys. Lett.*, vol. 114, no. 7, 2019, Art. no. 071104.
- [23] T. Van Vaerenbergh *et al.*, "Cascadable excitability in microrings," *Opt. Exp.*, vol. 20, no. 18, pp. 20292–20308, 2012.
- [24] A. M. Yacomotti *et al.*, "Fast thermo-optical excitability in a two-dimensional photonic crystal," *Phys. Rev. Lett.*, vol. 97, no. 14, 2006, Art. no. 143904.
- [25] M. Romagnoli *et al.*, "Graphene-based integrated photonics for next-generation datacom and telecom," *Nature Rev. Mater.*, vol. 3, no. 10, pp. 392–414, 2018.
- [26] Y. Lecun, L. Bottou, Y. Bengio, and P. Haffner, "Gradient-based learning applied to document recognition," *Proc. IEEE*, vol. 86, no. 11, pp. 2278–2324, Nov. 1998.
- [27] K. Roy, A. Jaiswal, and P. Panda, "Towards spike-based machine intelligence with neuromorphic computing," *Nature*, vol. 575, no. 7784, pp. 607–617, 2019.
- [28] M. Pfeiffer and T. Pfeil, "Deep learning with spiking neurons: Opportunities and challenges," *Front. Neurosci.*, vol. 12, p. 774, 2018.
- [29] B. Krauskopf, K. Schneider, J. Sieber, S. Wiczorek, and M. Wolfrum, "Excitability and self-pulsations near homoclinic bifurcations in semiconductor laser systems," *Opt. Commun.*, vol. 215, no. 4–6, pp. 367–379, 2003.
- [30] M. Mohrle, U. Feister, J. Horner, R. Molt, and B. Sartorius, "Gigahertz self-pulsation in 1.5  $\mu\text{m}$  wavelength multisection DFB lasers," *IEEE Photon. Technol. Lett.*, vol. 4, no. 9, pp. 976–978, Sep. 1992.
- [31] J. L. Dubbeldam, B. Krauskopf, and D. Lenstra, "Excitability and coherence resonance in lasers with saturable absorber," *Phys. Rev. E*, vol. 60, no. 6, 1999, Art. no. 6580.
- [32] J. L. Dubbeldam and B. Krauskopf, "Self-pulsations of lasers with saturable absorber: Dynamics and bifurcations," *Opt. Commun.*, vol. 159, no. 4–6, pp. 325–338, 1999.
- [33] H. Wünsche, O. Brox, M. Radziunas, and F. Henneberger, "Excitability of a semiconductor laser by a two-mode homoclinic bifurcation," *Phys. Rev. Lett.*, vol. 88, no. 2, 2001, Art. no. 023901.
- [34] Z. G. Pan *et al.*, "Optical injection induced polarization bistability in vertical-cavity surface-emitting lasers," *Appl. Phys. Lett.*, vol. 63, no. 22, pp. 2999–3001, 1993.
- [35] H.-T. Peng, M. A. Nahmias, T. F. de Lima, A. N. Tait, and B. J. Shastri, "Neuromorphic photonic integrated circuits," *IEEE J. Sel. Topics Quantum Electron.*, vol. 24, no. 6, pp. 1–15, Nov./Dec. 2018, Art. no. 6101715.
- [36] B. J. Shastri, M. A. Nahmias, A. N. Tait, and P. R. Prucnal, "Simulations of a graphene excitable laser for spike processing," *Opt. Quantum Electron.*, vol. 46, no. 10, pp. 1353–1358, 2014.
- [37] S. Barland, O. Piro, M. Giudici, J. R. Tredicce, and S. Balle, "Experimental evidence of van der Pol-Fitzhugh-Nagumo dynamics in semiconductor optical amplifiers," *Phys. Rev. E*, vol. 68, Sep. 2003, Art. no. 036209. [Online]. Available: <https://link.aps.org/doi/10.1103/PhysRevE.68.036209>
- [38] S. Wiczorek, B. Krauskopf, and D. Lenstra, "Multipulse excitability in a semiconductor laser with optical injection," *Phys. Rev. Lett.*, vol. 88, Jan. 2002, Art. no. 063901. [Online]. Available: <https://link.aps.org/doi/10.1103/PhysRevLett.88.063901>
- [39] D. Goulding *et al.*, "Excitability in a quantum dot semiconductor laser with optical injection," *Phys. Rev. Lett.*, vol. 98, Apr. 2007, Art. no. 153903. [Online]. Available: <https://link.aps.org/doi/10.1103/PhysRevLett.98.153903>
- [40] W. Coomans, S. Beri, G. V. D. Sande, L. Gelens, and J. Danckaert, "Optical injection in semiconductor ring lasers," *Phys. Rev. A*, vol. 81, Mar. 2010, Art. no. 033802. [Online]. Available: <https://link.aps.org/doi/10.1103/PhysRevA.81.033802>
- [41] L. Gelens *et al.*, "Excitability in semiconductor microring lasers: Experimental and theoretical pulse characterization," *Phys. Rev. A*, vol. 82, no. 6, 2010, Art. no. 063841.
- [42] K. Alexander, T. Van Vaerenbergh, M. Fiers, P. Mechet, J. Dambre, and P. Bienstman, "Excitability in optically injected microdisk lasers with phase controlled excitatory and inhibitory response," *Opt. Exp.*, vol. 21, no. 22, pp. 26182–26191, 2013.
- [43] B. Kelleher, C. Bonatto, G. Huyet, and S. Hegarty, "Excitability in optically injected semiconductor lasers: Contrasting quantum-well-and quantum-dot-based devices," *Phys. Rev. E*, vol. 83, no. 2, 2011, Art. no. 026207.
- [44] G. J. Spühler *et al.*, "Experimentally confirmed design guidelines for passively Q-switched microchip lasers using semiconductor saturable absorbers," *J. Opt. Soc. Amer. B*, vol. 16, no. 3, pp. 376–388, Mar. 1999. [Online]. Available: <http://josab.osa.org/abstract.cfm?URI=josab-16-3-376>
- [45] M. A. Larotonda, A. Hnilo, J. M. Mendez, and A. M. Yacomotti, "Experimental investigation on excitability in a laser with a saturable absorber," *Phys. Rev. A*, vol. 65, no. 3, 2002, Art. no. 033812.
- [46] F. Selmi, R. Braive, G. Beaudoin, I. Sagnes, R. Kuszelewicz, and S. Barbay, "Relative refractory period in an excitable semiconductor laser," *Phys. Rev. Lett.*, vol. 112, no. 18, 2014, Art. no. 183902.
- [47] W. Liu *et al.*, "A wavelength tunable optical buffer based on self-pulsation in an active microring resonator," *J. Lightw. Technol.*, vol. 34, no. 14, pp. 3466–3472, 2016.
- [48] M. Först *et al.*, "High-speed all-optical switching in ion-implanted silicon-on-insulator microring resonators," *Opt. Lett.*, vol. 32, no. 14, pp. 2046–2048, 2007.
- [49] C. Huang Prucnal *et al.*, "Programmable silicon photonic optical threshold," *IEEE Photon. Technol. Lett.*, vol. 31, no. 22, pp. 1834–1837, Nov. 2019.
- [50] C. Huang, A. Jha, T. F. De Lima, A. N. Tait, B. J. Shastri, and P. R. Prucnal, "On-chip programmable nonlinear optical signal processor and its applications," *IEEE J. Sel. Topics Quantum Electron.*, vol. 27, no. 2, pp. 1–11, Mar./Apr. 2021, Art. no. 6100211.
- [51] Q. Lin, O. J. Painter, and G. P. Agrawal, "Nonlinear optical phenomena in silicon waveguides: Modeling and applications," *Opt. Exp.*, vol. 15, no. 25, pp. 16604–16644, 2007.
- [52] C. Huang, T. F. De Lima, A. Jha, S. Abbaslou, A. N. Tait, B. J. Shastri, and P. R. Prucnal, "Programmable silicon photonic optical threshold," *IEEE Photonics Technology Letters*, vol. 31, no. 22, pp. 1834–1837, 2019.
- [53] A. Jha, C. Huang, T. F. de Lima, and P. R. Prucnal, "High-speed all-optical thresholding via carrier lifetime tunability," *Opt. Lett.*, vol. 45, no. 8, pp. 2287–2290, 2020.
- [54] V. G. Ataloglou, T. Christopoulos, and E. E. Kriezis, "Nonlinear coupled-mode-theory framework for graphene-induced saturable absorption in nanophotonic resonant structures," *Phys. Rev. A*, vol. 97, no. 6, 2018, Art. no. 063836.
- [55] S. Chen, L. Zhang, Y. Fei, and T. Cao, "Bistability and self-pulsation phenomena in silicon microring resonators based on nonlinear optical effects," *Opt. Exp.*, vol. 20, no. 7, pp. 7454–7468, 2012.
- [56] T. Uesugi, B.-S. Song, T. Asano, and S. Noda, "Investigation of optical nonlinearities in an ultra-high-Q Si nanocavity in a two-dimensional photonic crystal slab," *Opt. Exp.*, vol. 14, no. 1, pp. 377–386, Jan. 2006. [Online]. Available: <http://www.opticsexpress.org/abstract.cfm?URI=oe-14-1-377>
- [57] N. Vermeulen *et al.*, "Negative Kerr nonlinearity of graphene as seen via chirped-pulse-pumped self-phase modulation," *Phys. Rev. Appl.*, vol. 6, no. 4, 2016, Art. no. 044006.
- [58] D. Chatzidimitriou, A. Ptilakis, and E. E. Kriezis, "Rigorous calculation of nonlinear parameters in graphene-comprising waveguides," *J. Appl. Phys.*, vol. 118, no. 2, 2015, Art. no. 023105.
- [59] A. D. Bristow, N. Rotenberg, and H. M. Van Driel, "Two-photon absorption and Kerr coefficients of silicon for 850–2200 nm," *Appl. Phys. Lett.*, vol. 90, no. 19, 2007, Art. no. 191104.
- [60] E. Dremetsika *et al.*, "Measuring the nonlinear refractive index of graphene using the optical Kerr effect method," *Opt. Lett.*, vol. 41, no. 14, pp. 3281–3284, 2016.
- [61] A. Marini, J. Cox, and F. G. De Abajo, "Theory of graphene saturable absorption," *Phys. Rev. B*, vol. 95, no. 12, 2017, Art. no. 125408.

- [62] R. Soref and B. Bennett, "Electrooptical effects in silicon," *IEEE J. Quantum Electron.*, vol. 23, no. 1, pp. 123–129, Jan. 1987.
- [63] E. M. Izhikevich, "Resonate-and-fire neurons," *Neural Netw.*, vol. 14, no. 6–7, pp. 883–894, 2001.
- [64] M. Brunstein, A. M. Yacomotti, I. Sagnes, F. Raineri, L. Bigot, and A. Levenson, "Excitability and self-pulsing in a photonic crystal nanocavity," *Phys. Rev. A*, vol. 85, no. 3, 2012, Art. no. 031803.
- [65] E. M. Izhikevich, N. S. Desai, E. C. Walcott, and F. C. Hoppensteadt, "Bursts as a unit of neural information: Selective communication via resonance," *Trends Neurosci.*, vol. 26, no. 3, pp. 161–167, 2003.
- [66] K. Van Gasse, R. Wang, and G. Roelkens, "27 dB gain III-V-on-silicon semiconductor optical amplifier with > 17 dBm output power," *Opt. Exp.*, vol. 27, no. 1, pp. 293–302, 2019.
- [67] M. Brunstein, A. M. Yacomotti, I. Sagnes, F. Raineri, L. Bigot, and A. Levenson, "Excitability and self-pulsing in a photonic crystal nanocavity," *Phys. Rev. A*, vol. 85, p. 031803(R) (2012).
- [68] B. Romeira, J. Javaloyes, C. N. Ironside, J. M. Figueiredo, S. Balle, and O. Piro, "Excitability and optical pulse generation in semiconductor lasers driven by resonant tunneling diode photo-detectors," *Opt. Exp.*, vol. 21, no. 18, pp. 20931–20940, 2013.
- [69] A. Hurtado, A. Quirce, A. Valle, L. Pesquera, and M. J. Adams, "Nonlinear dynamics induced by parallel and orthogonal optical injection in 1550 nm vertical-cavity surface-emitting lasers (VCSELs)," *Opt. Exp.*, vol. 18, no. 9, pp. 9423–9428, 2010.
- [70] H. D. Thacker *et al.*, "Flip-chip integrated silicon photonic bridge chips for sub-picojoule per bit optical links," in *Proc. IEEE 60th Electron. Compon. Technol. Conf. (ECTC)*, 2010, pp. 240–246.
- [71] P. Kik and A. Polman, "Erbium-doped optical-waveguide amplifiers on silicon," *MRS Bull.*, vol. 23, no. 4, pp. 48–54, 1998.
- [72] J. H. Lee, T. Delbruck, and M. Pfeiffer, "Training deep spiking neural networks using backpropagation," *Front. Neurosci.*, vol. 10, p. 508, 2016.
- [73] P. U. Diehl, D. Neil, J. Binas, M. Cook, S.-C. Liu, and M. Pfeiffer, "Fast-classifying, high-accuracy spiking deep networks through weight and threshold balancing," in *Proc. Int. Joint Conf. Neural Netw.*, 2015, pp. 1–8.
- [74] A. Sengupta, Y. Ye, R. Wang, C. Liu, and K. Roy, "Going deeper in spiking neural networks: VGG and residual architectures," *Front. Neurosci.*, vol. 13, p. 95, 2019.
- [75] J. A. Pérez-Carrasco *et al.*, "Mapping from frame-driven to frame-free event-driven vision systems by low-rate rate coding and coincidence processing-application to feedforward ConvNets," *IEEE Trans. Pattern Anal. Mach. Intell.*, vol. 35, no. 11, pp. 2706–2719, Nov. 2013.
- [76] M. Abadi *et al.*, "Tensorflow: A system for large-scale machine learning," in *Proc. 12th USENIX Symp. Oper. Syst. Des. Implement.*, 2016, pp. 265–283.
- [77] A. Paszke *et al.*, "Pytorch: An imperative style, high-performance deep learning library," in *Proc. 33rd Int. Conf. Neural Inf. Process. Syst.*, 2019, pp. 8026–8037.
- [78] I. Chakraborty, G. Saha, and K. Roy, "Photonic in-memory computing primitive for spiking neural networks using phase-change materials," *Phys. Rev. Appl.*, vol. 11, no. 1, 2019, Art. no. 014063.
- [79] M. Hejda, J. Robertson, J. Bueno, J. A. Alanis, and A. Hurtado, "Neuromorphic encoding of image pixel data into rate-coded optical spike trains with a photonic VCSEL-neuron," *APL Photon.*, vol. 6, no. 6, 2021, Art. no. 060802.
- [80] F. Ponulak and A. Kasiński, "Supervised learning in spiking neural networks with resume: Sequence learning, classification, and spike shifting," *Neural Comput.*, vol. 22, no. 2, pp. 467–510, 2010.
- [81] R. Gütiğ and H. Sompolinsky, "The tempotron: A neuron that learns spike timing-based decisions," *Nature Neurosci.*, vol. 9, no. 3, pp. 420–428, 2006.
- [82] M. P. Fok, Y. Tian, D. Rosenbluth, and P. R. Prucnal, "Pulse lead/lag timing detection for adaptive feedback and control based on optical spike-timing-dependent plasticity," *Opt. Lett.*, vol. 38, no. 4, pp. 419–421, 2013.
- [83] Z. Song, S. Xiang, Z. Ren, G. Han, and Y. Hao, "Spike sequence learning in a photonic spiking neural network consisting of VCSELs-SA with supervised training," *IEEE J. Sel. Topics Quantum Electron.*, vol. 26, no. 5, pp. 1–9, Sep./Oct. 2020, Art. no. 1700209.
- [84] S. Xiang, Y. Zhang, J. Gong, X. Guo, L. Lin, and Y. Hao, "STDP-based unsupervised spike pattern learning in a photonic spiking neural network with VCSELs and VCSOs," *IEEE J. Sel. Topics Quantum Electron.*, vol. 25, no. 6, pp. 1–9, Nov./Dec. 2019, Art. no. 1700109.
- [85] S. Xiang *et al.*, "Computing primitive of fully VCSEL-based all-optical spiking neural network for supervised learning and pattern classification," *IEEE Trans. Neural Netw. Learn. Syst.*, vol. 32, no. 6, pp. 2494–2505, Jun. 2021.
- [86] S. M. Bohte, J. N. Kok, and J. A. La Poutré, "SpikeProp: Backpropagation for networks of spiking neurons," in *Proc. ESANN*, 2000, vol. 48, pp. 419–424.
- [87] N. Anwani and B. Rajendran, "Normad - normalized approximate descent based supervised learning rule for spiking neurons," in *Proc. Int. Joint Conf. Neural Netw.*, 2015, pp. 1–8.
- [88] H. Hazan *et al.*, "BindsNet: A machine learning-oriented spiking neural networks library in Python," *Front. Neuroinform.*, vol. 12, pp. 2494–2505, 2018. [Online]. Available: <https://www.frontiersin.org/article/10.3389/fninf.2018.00089>
- [89] R. Toole and M. P. Fok, "Photonic implementation of a neuronal algorithm applicable towards angle of arrival detection and localization," *Opt. Exp.*, vol. 23, no. 12, pp. 16133–16141, 2015.
- [90] Q. Ren, Y. Zhang, R. Wang, and J. Zhao, "Optical spike-timing-dependent plasticity with weight-dependent learning window and reward modulation," *Opt. Exp.*, vol. 23, no. 19, pp. 25247–25258, 2015.
- [91] S. Xiang *et al.*, "Numerical implementation of wavelength-dependent photonic spike timing dependent plasticity based on VCSEA," *IEEE J. Quantum Electron.*, vol. 54, no. 6, pp. 1–7, Dec. 2018, Art. no. 8100107.
- [92] C. Mesaritakis, M. Skontranis, G. Sarantoglou, and A. Bogris, "Micro-ring-resonator based passive photonic spike-time-dependent-plasticity scheme for unsupervised learning in optical neural networks," in *Proc. Opt. Fiber Commun. Conf. Exhibit.*, 2020, pp. 1–3.
- [93] P. Falez, P. Tirilly, I. M. Bilasco, P. Devienne, and P. Boulet, "Unsupervised visual feature learning with spike-timing-dependent plasticity: How far are we from traditional feature learning approaches?," *Pattern Recognit.*, vol. 93, pp. 418–429, 2019.
- [94] A. Amir *et al.*, "A low power, fully event-based gesture recognition system," in *Proc. IEEE Conf. Comput. Vision Pattern Recognit.*, 2017, pp. 7388–7397.
- [95] C. Mesaritakis, M. Skontranis, G. Sarantoglou, and A. Bogris, "Micro-ring-resonator based passive photonic spike-time-dependent-plasticity scheme for unsupervised learning in optical neural networks," *2020 Optical Fiber Communications Conference and Exhibition (OFC) 2020*, pp. 1–3.
- [96] I. Obeid and P. Wolf, "Evaluation of spike-detection algorithms for a brain-machine interface application," *IEEE Trans. Biomed. Eng.*, vol. 51, no. 6, pp. 905–911, Jun. 2004.
- [97] R. Lent, "Resource selection in cognitive networks with spiking neural networks," *IEEE Trans. Cogn. Commun. Netw.*, vol. 4, no. 4, pp. 860–868, Dec. 2018.

**Aashu Jha** received the B.S. degree in physics and math from Bates College, Lewiston, ME, USA, in 2017, and the M.A. degree in electrical engineering in 2019 from Princeton University, Princeton, NJ, USA, where she is currently working toward the Ph.D. degree advised by Prof Paul R. Prucnal. Her current research interests include nonlinear optics, optical signal processing, neuromorphic photonics, and photonic integrated circuits.

**Chaoran Huang** received the B.Eng. degree from the Huazhong University of Science and Technology, Wuhan, China in 2012, and the Ph.D. degree from the Chinese University of Hong Kong (CUHK), Hong Kong, in 2016. Before joining CUHK, she was a Postdoctoral Research Fellow with Princeton University, Princeton, NJ, USA, from 2017 to 2021. She has authored more than 40 peer-reviewed research papers, three book chapters, and one U.S. patent. Her research interests include silicon photonics, photonic integrated circuits, and nonlinear optics, serving applications, including neuromorphic computing, computing security, real-time information processing, and optical interconnects. Her current research focuses on developing neuromorphic photonic platforms, including novel devices, photonic integrated circuits, and complementary algorithms, for high-performance AI computing. She is a TPC member of several international conferences and is a frequent reviewer for different journals in IEEE, OSA, and Nature Publishing Group. She was the recipient of the 2019 Rising Stars Women in Engineering Asia, and was nominated by Princeton University to compete for Blavatnik Regional Awards for Young Scientists.

**Hsuan-Tung Peng** received the Honors B.Eng. (with distinction), M.Eng., and Ph.D. degrees in electrical engineering (photonics) from McGill University, Montreal, QC, Canada, in 2005, 2007, and 2012, respectively, the B.S. degree in physics from National Taiwan University, Taipei, Taiwan, in 2015, and the M.A. degree in electrical engineering in 2018 from Princeton University, Princeton, NJ, USA, where he is currently working toward the Ph.D. degree. He is currently an Assistant Professor of engineering physics with Queen's University, Kingston, ON, Canada, and a Faculty Affiliate with the Vector Institute for Artificial Intelligence, Canada. He was an NSERC and Banting Postdoctoral Fellow (during 2012–2016) and an Associate Research Scholar (during 2016–2018) with Princeton University. He has authored or coauthored more than 70 journal articles and 100 conference proceedings, seven book chapters, and given more than 60 invited talks and lectures, including five keynotes and three tutorials. He is the coauthor of the book *Neuromorphic Photonics* (Taylor & Francis, CRC Press, 2017), a term he helped coin. His research interests include silicon photonics, photonic integrated circuits, neuromorphic computing, and machine learning. His current research interests include neuromorphic photonics, photonic integrated circuits, and optical signal processing.

**Bhavin Shastri** (Senior Member, IEEE) was the recipient of the 2022 SPIE Early Career Achievement Award and 2020 IUPAP Young Scientist Prize in Optics for his pioneering contributions to neuromorphic photonics from the ICO. He is a Senior Member of Optica (formerly OSA), was the recipient of the 2014 Banting Postdoctoral Fellowship from the Government of Canada, 2012 D. W. Ambridge Prize for the top graduating Ph.D. student at McGill, IEEE Photonics Society 2011 Graduate Student Fellowship, 2011 NSERC Postdoctoral Fellowship, 2011 SPIE Scholarship in Optics and Photonics, 2008 NSERC Alexander Graham Bell Canada Graduate Scholarship, including the Best Student Paper Awards at the 2014 IEEE Photonics Conference, 2010 IEEE Midwest Symposium on Circuits and Systems, 2004 IEEE Computer Society Lance Stafford Larson Outstanding Student Award, and 2003 IEEE Canada Life Member Award.

**Paul R. Prucnal** (Life Fellow, IEEE) received the A.B. degree in mathematics and physics (*summa cum laude*) from Bowdoin College, Brunswick, ME, USA, and the M.S., M.Phil. and Ph.D. degrees in electrical engineering from Columbia University, New York, NY, USA. After his Doctorate, he joined the faculty with Columbia University, where he is/was a Member of Columbia Radiation Laboratory, he performed groundbreaking work in OCDMA and self-routed photonic switching. In 1988, he joined the faculty with Princeton University, Princeton, NJ, USA. His research on optical CDMA initiated a new research field in which more than 1000 papers have since been published, exploring applications ranging from information security to communication speed and bandwidth. In 1993, he invented the Terahertz Optical Asymmetric Demultiplexer, the first optical switch capable of processing terabit per second pulse trains. He is the author of the book *Neuromorphic Photonics* and the Editor of the book *Optical Code Division Multiple Access: Fundamentals and Applications*. He has authored or coauthored more than 350 journal articles and book chapters and holds 28 U.S. patents. He was an Area Editor of the IEEE TRANSACTIONS ON COMMUNICATIONS. He is a Fellow of the Optical Society of America and National Academy of Inventors, and a Member of honor societies, including Phi Beta Kappa and Sigma Xi. He was the recipient of the 1990 Rudolf Kingslake Medal for his paper entitled Self-routing photonic switching with optically-processed control, Gold Medal from the Faculty of Mathematics, Physics and Informatics at the Comenius University, for leadership in the field of Optics 2006 and multiple teaching awards at Princeton, including the E-Council Lifetime Achievement Award for Excellence in Teaching, School of Engineering and Applied Science Distinguished Teacher Award, and President's Award for Distinguished Teaching. He has been instrumental in founding the field of Neuromorphic Photonics and developing the photonic neuron, a high-speed optical computing device modeled on neural networks, and integrated optical circuits to improve wireless signal quality by cancelling radio interference.